Appl Phys B (2009) 94: 403–409
DOI 10.1007/s00340-008-3352-4

Applied Physics B
Lasers and Optics

Linear optimal control for tracking a single fluorescent particle in a confocal microscope

S.B. Andersson · T. Sun

Received: 13 September 2008 / Revised version: 6 December 2008 / Published online: 23 December 2008

Abstract We study the problem of localizing and tracking in a confocal laser scanning microscope a single fluorescent particle diffusing in three dimensions. The position of the particle is estimated from a collection of intensity measurements using a novel analytical algorithm. This estimator is then combined with a tracking algorithm based on a linear quadratic Gaussian controller to steer the detection volume of the microscope and follow the molecule. The feasibility of the approach is demonstrated through numerical simulations. These results indicate that, in such a system, tracking in three dimensions of a particle moving with a diffusion constant larger than 1 $\mu m^2/s$ is possible without the need for additional sensors or lasers.

PACS 87.64.mk · 87.64.kv · 87.80.Nj

1 Introduction

The ability to follow the dynamics of a single fluorescent particle has become a vital tool in molecular biology. The applications of single particle tracking techniques are wide ranging and include, among many others, the study of the process of infection by an influenza virus [1], the dynamics of molecular motors such as kinesin and dynein [2], and the motion of RNA molecules in bacterial cells [3, 4]. The range of applications of single-molecule techniques continues to expand and further examples can be found in recent reviews [5, 6].

Most methods to date for single-particle tracking rely on the use of wide field fluorescence microscopy and CCD cameras. Individual molecules can be localized in an image frame with nanometer accuracy [7] and a temporal resolution on the order of a few milliseconds. This approach is generally limited to motion in the focal plane. To extend this to three dimensions, images at different axial positions can be acquired and these stacks analyzed as a function of time to determine three-dimensional trajectories. Doing so, however, reduces the temporal resolution to the range of seconds [8]. By de-focusing, limited tracking in the axial direction with a temporal resolution of 100 ms has been achieved [9].

Recently, several researchers have developed tracking controllers that steer the detection volume of a single or multi-photon confocal microscope to track a fluorescent particle. Many schemes are built around a modulation scheme originally introduced by Enderlein [10]. Under this approach, the detection volume is moved rapidly around a circle and the resulting fluctuations in the intensity of the fluorescence signal reveal the location of the source particle. Tracking is achieved by wrapping a controller around this signal [11–14]. Using a variation of this scheme, involving two excitation beams focused to different axial positions, three-dimensional tracking of quantum dots moving with diffusion coefficients of 20 $\mu m^2/s$ has been achieved [15]. Alternative approaches include using multiple detectors to generate feedback signals [16–18] and using estimation theory coupled with a nonlinear control algorithm [19]. An overview of the state of the art can be found in a recent review article of progress in single molecule tracking spectroscopy [20].

S.B. Andersson (✉) · T. Sun
Department of Mechanical Engineering, Boston University, Boston, MA 02215, USA
e-mail: sanderss@bu.edu

T. Sun
e-mail: tingsun@bu.edu

In this paper we design a linear controller to track a fluorescent particle diffusing in three dimensions. We do not move the focal point around a circle to generate estimates of the position. Rather, we utilize a novel algorithm developed by the authors [21, 22] that can determine the three-dimensional position of a fluorescent molecule from as few as four measurements. The location of these measurements is specified with respect to a common center. A tracking controller based on linear quadratic Gaussian theory is then designed to drive this center to the position of the fluorescent particle. Unlike other approaches for tracking in three dimensions, the scheme does not require an additional excitation laser nor additional detection hardware. It can be implemented on a variety of different actuators, including sample-actuated systems in which the sample is moved through the detection volume using a three-dimensional nanopositioning stage and beam-steering systems utilizing galvanometers or acousto-optic modulators to direct the excitation beam in the focal plane combined with a piezoelectric actuator to move either the objective or the sample along the optical axis.

This work focuses on trajectory generation and ignores the details of the dynamics of the actuators typically used to move the sample or to steer the beam. While control of piezoelectric actuators for both high speed and high precision is challenging, recent advances in the control of such devices have shown that nonlinearities such as hysteresis and creep can be overcome, allowing control at rates even beyond the resonant frequency of the device [23–25]. For the purposes of presenting the high-level algorithm discussed here, we therefore assume that a low-level controller is used that can drive the actuators to follow faithfully the trajectories produced by the tracking controller introduced in this paper.

2 System model

We model the motion of the fluorescent particle as a random walk in three dimensions. Let $x_m[k] \in \mathbb{R}^3$ denote the position of the molecule at time step k. Then

$$x_m[k+1] = x_m[k] + \sqrt{2D\Delta t}\, v[k], \tag{1}$$

where D is the diffusion constant, Δt is the duration of the time step, and $v[\cdot]$ is a zero-mean, unity-variance Gaussian white noise stochastic process.

At each time step we will collect a set of intensity measurements from a constellation of positions defined relative to a common point x_c. As discussed in Sect. 3, this collection of measurements will be used to generate an estimate of the position of the fluorescent particle. Noise in the measured intensities (primarily from background fluorescence and shot noise in the detectors) will propagate through the localization algorithm, yielding a stochastic estimate. For the purposes of control, we will model this as a direct measurement of the position of the fluorescent particle corrupted by noise,

$$y_m[k] = x_m[k] + w[k], \tag{2}$$

where $w[\cdot]$ is a zero-mean Gaussian white noise process with variance Σ_{ww}. The statistics of $w[\cdot]$ are determined by the estimator in Sect. 3.

The goal of the controller will be to drive the point x_c to track the fluorescent particle. Since we are free to determine x_c, we describe its evolution as

$$x_c[k+1] = x_c[k] - u[k], \tag{3}$$

where the sign on the input $u[\cdot]$ was chosen to yield a positive sign in the error dynamics in (5) below. Define the error as

$$e[k] = x_m[k] - x_c[k]. \tag{4}$$

The error dynamics are then given by

$$\begin{aligned} e[k+1] &= x_m[k+1] - x_c[k+1] \\ &= x_m[k] - x_c[k] + u[k] + \sqrt{2D\Delta t}\, v[k] \\ &= e[k] + u[k] + \sqrt{2D\Delta t}\, v[k]. \end{aligned} \tag{5}$$

Similarly, we define the measurement of the error as $y_e = y_m - x_c$. Using (2) and (4), we have

$$y_e[k] = e[k] + w[k]. \tag{6}$$

Tracking is achieved by driving the error system defined by (5) and (6) to zero.

3 Position estimation

In a confocal or multi-photon setup, intensity measurements are obtained sequentially. The control-loop time, and thus the temporal resolution, of a feedback tracking scheme is directly related to the time it takes to generate an estimate of the position of the molecule. Several algorithms exist for accurate localization in a wide-field image of a sub-diffraction-limit fluorescent particle, with Gaussian fitting being one of the most effective [7, 26]. Such approaches are typically limited to two dimensions and require a substantial amount of data for accurate results and are therefore not well suited for real-time feedback control in a confocal microscope. Schemes that utilize fluctuations in the measured intensity as the excitation source is moved rapidly around a known pattern still require a relatively large number of measurements collected over multiple cycles of the detection volume around that pattern [12], although the signal can be

processed using a lock-in amplifier to quickly provide the estimate [15].

In this work we take advantage of an algorithm previously developed by the authors [21, 22]. The algorithm, inspired by the Bancroft algorithm used for determining the position of a receiver in the Global Positioning System (GPS), views each intensity measurement as yielding a measurement of the *range* to the fluorescent particle. Thus, in the absence of noise, a single measurement generates a sphere, centered on where that measurement was taken, on which the fluorescent particle must be. Two measurements produce two such spheres and the fluorescent particle must be on the intersection of the two. Since the maximum intensity is not known a priori, four such measurements are necessary to generate a unique solution in three dimensions. Additional measurements reduce the error due to noise. While similar in spirit to approaches that utilize additional detectors to sense the position of the fluorescent particle [16, 18], this scheme does not require any additional hardware.

We give here a brief outline of the algorithm; details can be found in [21]. The measured intensity I_i at a point (x_i, y_i, z_i) due to a fluorescent particle at (x_0, y_0, z_0) is modeled according to a Gaussian function [8]

$$I_i = m \exp\left(-\frac{(x_i - x_0)^2}{2\sigma_x^2} - \frac{(y_i - y_0)^2}{2\sigma_y^2} - \frac{(z_i - z_0)^2}{2\sigma_z}\right) + \eta_\mathrm{B} + \eta_\mathrm{s}. \tag{7}$$

Here η_B denotes noise due to background fluorescence and η_s denotes shot noise in the detectors. The spreads σ_x, σ_y, and σ_z can either be estimated using expressions for the full-width at half-maximum of the point-spread function or measured experimentally. Through appropriate scaling of the axes, we can without loss of generality assume that these are all equal (see [21]). Collecting a set of n intensity measurements from different locations in space leads to a linear system of the form

$$B\begin{pmatrix} x_0 \\ y_0 \\ z_0 \\ b \end{pmatrix} = \alpha + \lambda e, \tag{8}$$

where B is a (known) $n \times 4$ matrix collecting the positions of the measurements, α is a (known) $n \times 1$ vector generated from the intensity measurements I_i and the positions at which those measurements were collected, e is an $n \times 1$ vector of all ones, λ is an unknown scalar depending on the position of the source molecule, (x_0, y_0, z_0), and b is an unknown scalar depending on the maximum intensity of the particle. Applying the Moore–Penrose inverse [27] to (8) and then pre-multiplying by a matrix to isolate the position (x_0, y_0, z_0) on the left-hand side, we find an analytical solution given by

$$(x_0 \quad y_0 \quad z_0)^\mathrm{T} = QB^\dagger\alpha, \tag{9}$$

where $B^\dagger = (B^\mathrm{T}B)^{-1}B^\mathrm{T}$ is the Moore–Penrose inverse and

$$Q = \begin{pmatrix} 1 & 0 & 0 & 0 \\ 0 & 1 & 0 & 0 \\ 0 & 0 & 1 & 0 \end{pmatrix}.$$

Note that there are four unknowns in the system (8). As a result at least four measurements from different locations in space are needed to ensure that B is full rank. Additional measurements reduce the variance of the estimator. Regardless of the number of measurements, the algorithm requires only matrix multiplications and the inversion of a 4×4 matrix.

4 Optimal LQG controller design

Consider a discrete-time linear system of the form

$$x_{k+1} = Ax_k + Bu_k + v_k, \tag{10a}$$

$$y_k = Cx_k + w_k, \tag{10b}$$

where $v[\cdot]$ is a zero-mean input noise process with covariance Σ_{vv} and w_k is a zero-mean measurement noise process with covariance Σ_{ww}. The linear quadratic Gaussian (LQG) controller combines a linear quadratic regulator (LQR) that minimizes a quadratic cost function of the state with a Kalman filter that produces the minimum-variance estimate of the state [28].

We apply this control framework to the linear model derived in Sect. 2 of the evolution of the error:

$$e[k+1] = e[k] + u[k] + \sqrt{2D\Delta t}v[k], \tag{11a}$$

$$y_e[k] = e[k] + w[k]. \tag{11b}$$

4.1 LQR controller

An LQR controller seeks to minimize a cost function of the form

$$J = \sum_0^\infty \left(e^\mathrm{T}[k]Qe[k] + u^T[k]Ru[k]\right), \tag{12}$$

where Q is a weighting matrix on the cost of the error and R is a weighting matrix on the cost of the control. We take

$$Q = a\begin{bmatrix} 1 & 0 & 0 \\ 0 & b & 0 \\ 0 & 0 & c \end{bmatrix}, \qquad R = d\begin{bmatrix} 1 & 0 & 0 \\ 0 & 1 & 0 \\ 0 & 0 & 1 \end{bmatrix}, \tag{13}$$

where we allow the weights in the y- and z-directions to be tuned based on the beam waists in those directions. The choice of d allows us to alter the relative weight of the cost

of control against the need to drive the error to zero. According to standard infinite-horizon LQR theory, the optimal linear feedback controller has the form

$$u[k] = -Ke[k], \tag{14}$$

where the feedback gain for the system in (11) is

$$K = (P + R)^{-1} P. \tag{15}$$

Here P is the solution to the discrete-time algebraic Riccati equation, which, for the system (11), takes the form

$$Q = P(R + P)^{-1} P. \tag{16}$$

Given the diagonal weighting matrices (13), the above equations can be explicitly solved, yielding

$$K = \begin{bmatrix} \frac{a+\sqrt{a^2+4ad}}{a+d+\sqrt{a^2+4ad}} & 0 & 0 \\ 0 & \frac{b+\sqrt{b^2+4bd}}{b+d+\sqrt{b^2+4bd}} & 0 \\ 0 & 0 & \frac{c+\sqrt{c^2+4cd}}{c+d+\sqrt{c^2+4cd}} \end{bmatrix}. \tag{17}$$

In the error system defined by (11), the state itself is not available and thus cannot be used in the optimal control (14). The LQG controller replaces the state feedback by an estimate of the state generated by a Kalman filter.

4.2 Kalman filter

The Kalman filter is a minimum-variance, unbiased filter. In one standard formulation, it consists of a prediction phase in which the system model is used to propagate the mean and covariance of the system state, followed by an update phase in which the estimate is refined using the current measurement. Let $\hat{e}[k+1|k]$ and $P[k+1|k]$ denote the mean and covariance of the error at time $k+1$ using information up to time k. The mean and covariance are propagated from the previous values according to

$$\hat{e}[k+1|k] = \hat{e}[k|k] + u[k], \tag{18a}$$

$$P[k+1|k] = P[k|k] + 2D\Delta t\mathbb{I}, \tag{18b}$$

where $\mathbb{I}$ is a 3×3 identity matrix. They are then updated based on the new measurement $y[k+1]$ according to

$$\hat{e}[k+1|k+1] = \hat{e}[k+1|k] + G[k+1]z[k+1], \tag{19a}$$

$$P[k+1|k+1] = \big(\mathbb{I} - G[k+1]\big)P[k+1|k], \tag{19b}$$

where the Kalman gain is

$$G[k+1] = P[k+1|k]\big(P[k+1|k] + \Sigma_{ww}\big)^{-1} \tag{20}$$

and the innovations, $z[k+1]$, are the error between the actual and predicted values of the measurement:

$$z[k+1] = y_e[k+1] - \hat{e}[k+1|k]. \tag{21}$$

Note that the evolution of the Kalman gain in (20) and of the covariance in (18b) and (19b) do not depend on the measurements. It can be shown that both converge to steady-state values G_∞ and P_∞. Because the filter defined by (18) and (19) is stable, any error in the initial conditions dies away. In practice, if no prior information on the initial error is known then the filter is typically initialized with $e[0|0] = 0$ and with $P[0|0] = P_\infty$.

5 Numerical simulations

In order to demonstrate the feasibility of the proposed approach and to provide guidance on choosing the number of measurements to use in the position-estimation step, we constructed a numerical simulation in the Matlab environment. The motion of a single diffusing particle fluorescing at a wavelength of $\lambda = 507$ nm (the emission wavelength of the enhanced green fluorescent protein (EGFP)) was simulated. The intensity measurements were modeled according to (7) with $\sigma_x = \sigma_y = 0.2155$ µm and $\sigma_z = 0.5818$ µm. These values were chosen according to the full-width at half-maximum (FWHM) corresponding to the first minimum of the intensity function in the three principal directions for a 1.2 N.A. objective lens (see e.g. [29]). The background fluorescence rate was set to 1 photon/ms while the source molecule was set to a fluorescence rate of 50 photons/ms. The initial position of the fluorescent particle was set to be the origin. The position of the particle was updated according to (1) after each measurement; thus, the particle moved multiple times inside each control-loop period.

The standard deviation of the position estimator defined by the fluoroBancroft algorithm was set to $\sigma_w = 100$ nm, yielding $\Sigma_w = \sigma_w^2\mathbb{I}$. Note that in the LQG controller, a small value of σ_w leads to a higher weight being given to each individual measurement. The value of 100 nm was chosen empirically. The weights for the LQR controller were selected somewhat arbitrarily as $a = b = c = 1$ and $d = 0.01$.

The measurement constellation was chosen through hand tuning to improve the tracking performance of the scheme. The constellation was defined by a grid centered on the current value of x_c (see Fig. 1). One unit in the grid was set to $d = 100$ nm and points were chosen in the order shown in the figure. That is, for an eight-measurement constellation, points indicated by 1–8 were used in each measurement cycle. Three points (points 6–8) were taken to be a distance of $2d = 200$ nm along the x-, y-, and z-axes, respectively, and are not shown in the figure.

In Fig. 2 we show a sample run in which a molecule is diffusing with $D = 0.5\ \mu m^2/s$. Six measurements were used to generate the position estimate. Each measurement was taken for 1 ms, leading to a control-loop time of 6 ms. The trajectory of the particle is shown in Fig. 2a, clearly indicating its diffusive behavior. Figure 2b shows the magnitude of the actual error between the position of the particle and the position of x_c while the errors in the individual axes are shown in Fig. 2c. Note that the tracking in the axial (z) direction was poorer than in the lateral directions. This arises from the larger value of σ_z, leading to poorer estimation in this direction. The mean of the error magnitude over this two-second run was 154 nm with a standard deviation of 66.9 nm. The mean of the measured intensity over the two-second run was 38 counts.

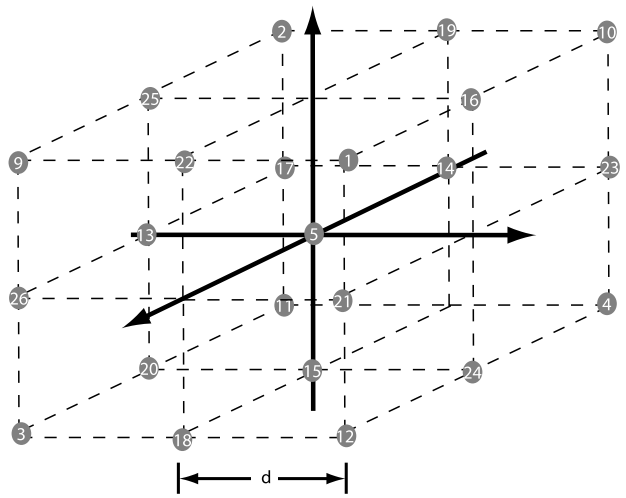

Fig. 1 The measurement constellation was defined by a grid with spacing of $d = 100$ nm. Three points were taken to be 200 nm away along the x-, y-, and z-axes and are not shown in this figure

5.1 Effect of number of measurements in position estimate

Increasing the number of measurements used in each position estimate has two competing effects. First, as the number of measurement points is increased, the accuracy of the fluoroBancroft estimation improves. This in turn leads to improved performance of the tracking algorithm. Second, as the number of measurement points is increased, the control-loop time also increases. The diffusing particle thus moves more during each control cycle. This reduces the performance of the tracking algorithm, since the fluoroBancroft estimator assumes that the particle is fixed during the measurement sequence.

To investigate the effect of using different numbers of measurements in each position estimate, we simulated a particle diffusing with a coefficient of $D = 0.5\ \mu m^2/s$ and fixed the measurement time to be 1 ms. The mean error and standard deviation over two seconds of tracking were determined as a function of the number of measurements used in each estimate (from four to 27). The results are shown in Fig. 3. There was a slight improvement in both the mean error and the standard deviation in the error as the number of measurements increased from four to five. As additional measurements were added, the performance degraded. Note that the results in this figure are only from successful runs in which the particle was tracked for the full two seconds. Above 20 measurements the assumption that the particle was fixed during the measurement sequence was poor and multiple runs were needed to track over the full two seconds.

5.2 Effect of measurement time

Increasing the measurement time for a fixed number of measurements also has two competing effects. First, a longer measurement time yields a larger signal to noise ratio. This

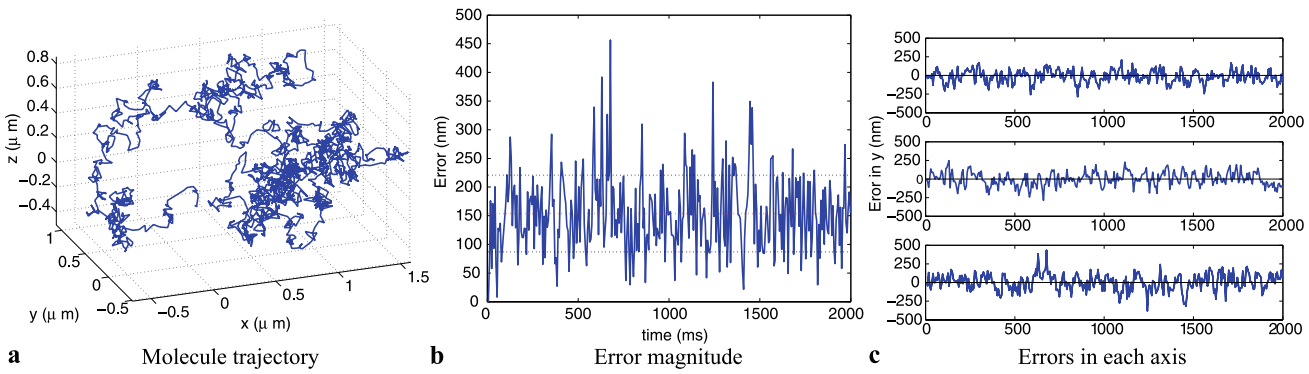

Fig. 2 Sample run of tracking a particle diffusing with $D = 0.5\ \mu m^2/ms$. Six measurements were used in the fluoroBancroft algorithm to generate an estimate of the position of the molecule. The control-loop time was $\Delta t = 6$ ms. As expected, the error in the axial direction was larger than in the lateral directions. The mean of the magnitude of the error throughout the run was 154 nm (*red dotted line*) with a standard deviation of 66.9 nm (*black dotted lines*)

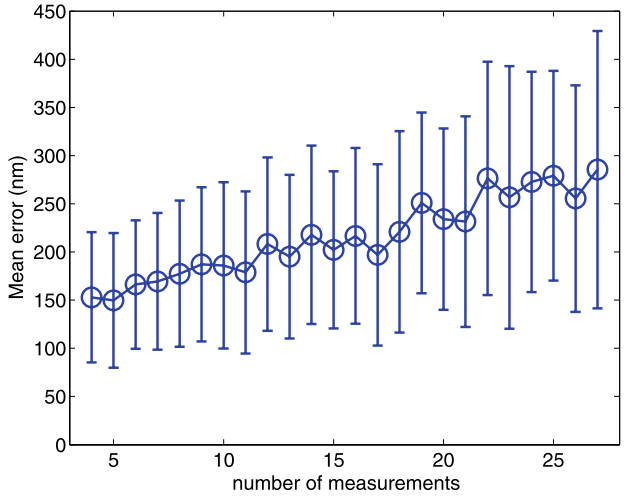

Fig. 3 Mean error over one second as a function of the number of measurements used in the position estimate. *Error bars* indicate the standard deviation in the error. The particle diffusion coefficient was $D = 0.5\ \mu m^2/s$ and the measurement time was 1 ms at each constellation point. The results indicate that best performance is achieved when fewer measurements are used

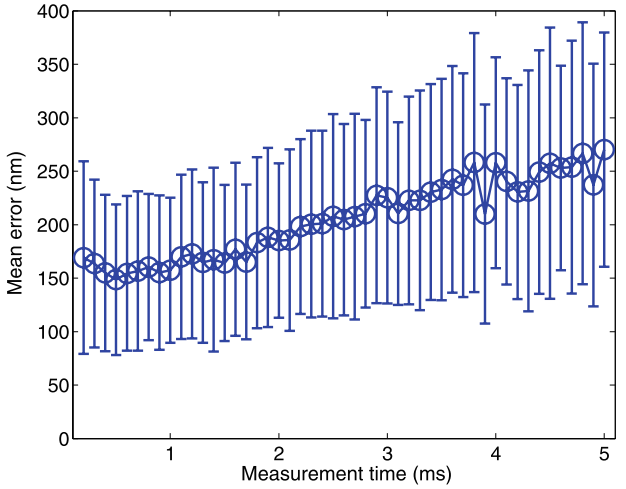

Fig. 4 Mean error over two seconds of tracking as a function of the amount of time spent on each measurement. The particle diffusion coefficient was $D = 0.5\ \mu m^2/s$ and five measurements were used in each measurement cycle. The accuracy improved as the measurement time increased from 0.2 to 0.5 ms and then remained relatively constant until approximately a 1-ms measurement time. After that the error increased approximately linearly

in turn increases the accuracy of the estimate of the position of the molecule produced by the fluoroBancroft algorithm. As this time is increased, however, the assumption that the particle is fixed becomes increasingly violated since the molecule is continually moving. To explore these competing effects, we simulated a particle diffusing with $D = 0.5\ \mu m^2/s$, fixed the number of measurements per update to five, and varied the measurement time from 0.2 to 5 ms. The mean error and standard deviation over two seconds of tracking as a function of the measurement time are shown in Fig. 4. The tracking performance improved slightly as the measurement time was increased from 0.2 to 0.5 ms and then began to degrade with increasing measurement time. As before, these results represent only successful runs. For measurement times above 4 ms, multiple trials were needed to yield a successful run.

5.3 Tracking limits

To investigate the performance of the algorithm as a function of the diffusion constant, simulations were performed in which the diffusion constant was varied from 10^{-9} to $10\ \mu m^2/s$. Based on the results of the earlier simulations, five measurements were used in each estimate. One run was done with the measurement time set to 1 ms and another with the measurement time set to 5 ms. Tracking was deemed successful if the particle was tracked for two seconds. The results are shown in Fig. 5.

With the shorter measurement time, tracking was successful up to $D = 2\ \mu m/s^2$. The mean error was constant for very small values of the diffusion constant, while, above

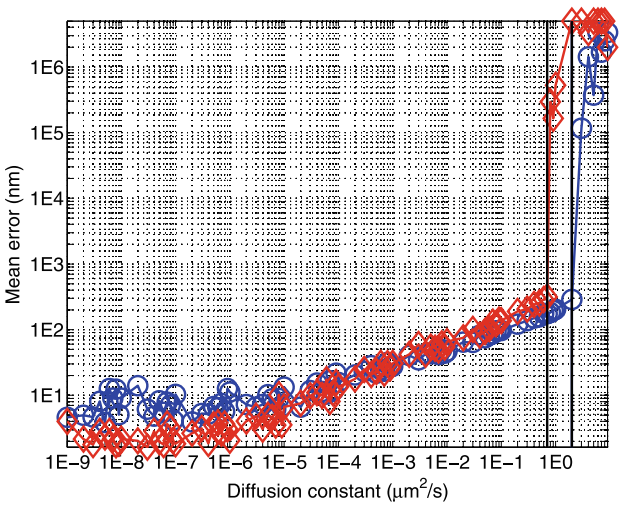

Fig. 5 Mean error over two seconds of tracking as a function of the diffusion coefficient. Five measurements were used in each measurement cycle. The *blue circles* represent a run with a measurement time of 1 ms while the red diamonds represent an integration time of 5 ms. Using the shorter measurement time, the scheme was able to track particles moving at up to $2\ \mu m^2/s$, while the longer measurement time was able to track up to $0.7\ \mu m^2/s$. For very small diffusion constants, the shorter measurement time is less accurate, with an average error of 7.9 nm across diffusion constants from 10^{-9} to $10^{-6}\ \mu m^2/s$, as compared to an average error of 3.6 nm when the longer measurement time was used. Note that the error at larger D indicates only that tracking was lost

$10^{-5}\ \mu m^2/s$, the error increased exponentially with increasing D until tracking failed. The same trend occurred for the longer measurement time, but tracking was successful only up to $D = 0.7\ \mu m^2/s$.

At very low values of D, the particle is essentially fixed and the tracking error reflects the estimation error in the fluoroBancroft algorithm. The average error across values of D lower than 10^{-5} $\mu m^2/s$ was 3.6 nm when the measurement time was 5 ms, as compared to 7.9 nm when the measurement time was 1 ms.

6 Conclusions

In this paper we described and numerically studied a scheme for tracking a single fluorescent particle in a confocal microscope. The approach couples a position estimator with a LQG regulator to achieve tracking. The simulation results are encouraging and suggest that tracking of molecules diffusing in three dimensions with diffusion constants larger than 1 $\mu m/s^2$ can be achieved using this scheme.

The simulations utilized a fixed measurement pattern that in practice would likely be replaced by a continuous sweep of the excitation source through a path defined by the desired measurement locations. The path should be chosen to optimize the accuracy of the position estimation as well as to ensure that the actuators can faithfully follow the trajectory. The optimal design of this path is an interesting and open question.

Acknowledgement This work has been supported in part by the National Science Foundation through Grant No. DBI-0649823.

References

1. H.P. Babcock, C. Chen, X. Zhuang, Biophys. J. **87**, 2749 (2004)
2. C. Kural, H. Kim, S. Syed, G. Goshima, V.I. Gelfand, P.R. Selvin, Science **308**, 1469 (2005)
3. I. Golding, J. Paulsson, S.M. Zawilski, E.C. Cox, Cell **123**, 1025 (2005)
4. C.C. Guet, L. Bruneaux, T.L. Min, D. Siegal-Gaskins, I. Figueroa, T. Emonet, P. Cluzel, Nucleic Acids Res. **36**, e73 (2008)
5. W.E. Moerner, Proc. Natl. Acad. Sci. USA **104**, 12596 (2007)
6. N.G. Walter, C.-Y. Huang, A.J. Manzo, M.A. Sobhy, Nat. Methods **5**, 475 (2008)
7. R.E. Thompson, D.R. Larson, W.W. Webb, Biophys. J. **82**, 2775 (2002)
8. D. Thomann, D.R. Rines, P.K. Sorger, G. Danuser, J. Microsc. **208**, 49 (2002)
9. M. Speidel, A. Jonáš, E.-L. Florin, Opt. Lett. **28**, 69 (2003)
10. J. Enderlein, Appl. Phys. B: Lasers Opt. **71**, 773 (2000)
11. V. Levi, Q. Ruan, K. Kis-Petikova, E. Gratton, Biochem. Soc. Trans. **31**, 997 (2003)
12. V. Levi, Q. Ruan, E. Gratton, Biophys. J. **88**, 2919 (2005)
13. A.J. Berglund, H. Mabuchi, Appl. Phys. B: Lasers Opt. **78**, 653 (2004)
14. A.J. Berglund, H. Mabuchi, Opt. Express **13**, 8069 (2005)
15. K. McHale, A.J. Berglund, H. Mabuchi, Nano Lett. **7**, 3535 (2007)
16. H. Cang, C.M. Wong, C.S. Xu, A.H. Rizvi, H. Yang, Appl. Phys. Lett. **88**, 223901 (2006)
17. H. Cang, C.S. Xu, D. Montiel, H. Yang, Opt. Lett. **32**, 2729 (2007)
18. G.A. Lessard, P.M. Goodwin, J.H. Werner, Appl. Phys. Lett. **91**, 224106 (2007)
19. S.B. Andersson, Appl. Phys. B: Lasers Opt. **80**, 809 (2005)
20. H. Cang, C.S. Xu, H. Yang, Chem. Phys. Lett. **457**, 285 (2008)
21. T. Sun, S.B. Andersson, in *Proc. Int. Conf. IEEE Engineering in Medicine and Biology Soc.* (2007), pp. 4181–4184
22. S.B. Andersson, Opt. Express **16**, 18714 (2008)
23. D. Croft, G. Shed, S. Devasia, J. Dyn. Syst. Meas. Control **123**, 35 (2001)
24. Y. Wu, Q. Zou, IEEE Trans. Control Syst. Technol. **15**, 936 (2007)
25. D.Y. Abramovitch, S. Hoen, R. Workman, in *Proc. American Control Conf.* (2008), pp. 2684–2689
26. M.K. Cheezum, W.F. Walker, W.H. Guilford, Biophys. J. **81**, 2378 (2001)
27. A. Ben-Israel, T.N.E. Greville, *Generalized Inverses: Theory and Applications*. Pure Appl. Math. (Wiley, New York, 1974)
28. B.D.O. Anderon, J.B. Moore, *Optimal Control: Linear Quadratic Methods* (Dover, New York, 2007)
29. S. Inoué, Foundations of confocal scanned imaging in light microscopy, in *Handbook of Biological Confocal Microscopy*, 3rd edn. Chap. 1 (Springer, Berlin, 2006), pp. 1–14